Physics in Medicine & Biology
J. Gomez-Tames *et al*
Post-Print Version
doi:10.1088/1361-6560/61/24/8825

Effect of Microscopic Modeling of Skin in Electrical and Thermal Analysis of Transcranial Direct Current Stimulation

Jose Gomez-Tames[1], Yukiya Sugiyama[1], Ilkka Laakso[2], Satoshi Tanaka[3], Soichiro Koyama[4], Norihiro Sadato[5,6], Akimasa Hirata[1]

1. Department of Computer Science and Engineering, Nagoya Institute of Technology
2. Aalto University, Espoo, Finland
3. Hamamatsu University School of Medicine, Hamamatsu, Japan.
4. Faculty of Rehabilitation, School of Health Sciences, Fujita Health University, Toyoake, Aichi, Japan
5. National Institute for Physiological Sciences, Okazaki, Japan
6. Department of Physiological Sciences, SOKENDAI (The Graduate University for Advanced Studies), Kanagawa, Japan

Corresponding author:

Akimasa Hirata

Nagoya Institute of Technology

ahirata@nitech.ac.jp

Physics in Medicine & Biology
J. Gomez-Tames *et al*
Post-Print Version
doi:10.1088/1361-6560/61/24/8825

Abstract

Transcranial direct current stimulation (tDCS) is a neuromodulation scheme where a small current is delivered to the brain via two electrodes attached to the scalp. The electrode design is an important topic for not only the efficacy but also for the safety of tDCS, because it may be related to skin lesions that are sometimes observed after stimulation. Previous computational models of tDCS have omitted the effects of microscopic structures in the skin and different soak conditions of the electrodes, and model validation has been limited. In this study, multiphysics and multiscale analysis are proposed to demonstrate the importance of microscopic modeling of the skin to clarify the effects of internal electric field and temperature elevation around the electrodes. The novel microscopic model of the skin layer considered the effect of saline/water penetration in the hair follicles and sweat ducts on the field distribution around the electrodes. The temperature elevation in the skin was then computed by solving the bioheat equation. Also, a multiscale model was introduced to account for macroscopic and microscopic tissues of the head and skin, which was validated by measurement of the head resistance during tDCS. As a result, the electric field in the microscopic model of the skin was less localized when the follicles/ducts were filled with saline instead of hair or tap water. The temperature elevation was also smaller for the case of saline than for the others. The saline, which may penetrate the hair follicles and sweat ducts, suppressed the field concentration around the electrodes. For conventional magnitudes of current injection and a head resistance less than 10 kΩ, the temperature elevation in the skin due to the saline-soaked electrodes was small, less than 0.1 °C, and unlikely to cause adverse thermal effects.

Physics in Medicine & Biology
J. Gomez-Tames *et al*
Post-Print Version
doi:10.1088/1361-6560/61/24/8825

1. Introduction

In the last decade, brain stimulation has attracted considerable attention of neuroscientists (e.g., (Nitsche *et al.*, 2008; Rossi *et al.*, 2009)). Among others, transcranial direct current stimulation (tDCS) is often applied to motor and cognitive research (Elsner *et al.*, 2013, 2015; Tanaka and Watanabe, 2009; Tanaka *et al.*, 2011). It is a neuromodulation scheme, wherein a small current (a few milliamperes) is delivered to the brain via two electrodes attached on the scalp. There have been many clinical studies reporting its potential efficacy in improving motor function (Webster *et al.*, 2006; Nitsche and Paulus, 2000; Roy *et al.*, 2014).

The electrode design is an important topic in tDCS, for not only the efficacy but also the safety evaluated by the current density distribution under the electrode (Nathan *et al.*, 1993; Bikson *et al.*, 2009; Minhas *et al.*, 2010). The volume conductor model, in which human tissues are expressed in terms of the measured conductivity, is often used to investigate the internal electric field (Datta *et al.*, 2009a; Parazzini *et al.*, 2011; Brunoni *et al.*, 2012; Wagner *et al.*, 2014; Noetscher *et al.*, 2014; Saturnino *et al.*, 2015; Laakso *et al.*, 2015). Most studies have evaluated the internal electric field in the brain to discuss the optimal electrode locations and design. In Saturnino *et al.* (2015), the low saline content (low conductivity) of the electrode is suggested to be useful for generating a homogeneous field around the electrode.

Adverse effects of tDCS have been reported since the 2000s, and mild pain and transient redness in the skin have been documented (Bikson *et al.*, 2009; Brunoni *et al.*, 2012; Loo *et al.*, 2011). It was reported that, during treatments of five days per week for a two- or three-week period, lesions appeared after a few days of treatment and continued to appear until the end of the treatment (Frank *et al.*, 2010; Palm *et al.*, 2008). The lesion size ranged from a few millimeters to 20 mm and was approximately proportional to the skin resistance. In these studies, the electrodes were soaked in tap water, instead of a saline solution, to suppress itching,

and an electroencephalogram was recorded immediately after the treatment. Mild redness in the hair follicles of the scalp was reported in Kasahara *et al.* (2011) for an injection current of 1 mA. Moreover, extensive data is summarized in (Poreisz *et al.*, 2007; Kuo *et al.*, 2014). Computational approach has shown possible causes of the adverse effect of current density distribution. The internal electric field in the skin was shown to be strong along the edges of the electrode (Miranda *et al.*, 2006; Minhas *et al.*, 2011). Moreover, the internal electric field in the skin of an anatomical head model was shown to be large for a typical electrode configuration but insufficient to induce temperature elevation causing a burning sensation (Datta *et al.*, 2009b). In these studies, the effect of soaking the electrodes in water was not considered, and in general, selecting electrodes and contact medium (Woods *et al.*, 2015) is inconsistent and not standardized. Also, the validation of the volume conductor model for tDCS is limited; one study compared the computed electrical potential with measurements (Bikson *et al.*, 2012); the resistance between the electrodes including the head is used as a metric when discussing side effects.

This study investigates for the first time a microscopic computational model of the skin by including stratum corneum, epidermis and dermis tissues with hair follicles and sweat ducts. Some microscopic discussion on skin modeling can be found in (Huclova *et al.*, 2011; Schmid *et al.*, 2013) for high and low frequency, respectively. The effect on the internal electric field and temperature elevation is computed around the electrodes of saline/water penetration in the hair follicles and sweat ducts during tDCS. In addition, multiscale simulations of the head were compared with experimental measurements in human participants to validate the proposed microscopic skin model by reproducing tDCS conditions in the experiment. A discussion on the side effects of tDCS is provided according to the computation of the internal field and the resultant temperature elevation as well as the importance of microscopic modeling of the skin.

Physics in Medicine & Biology
J. Gomez-Tames *et al*
Post-Print Version
doi:10.1088/1361-6560/61/24/8825

2. Model and methods

2.1. Participants

The participants were seven male volunteers 28.9 (mean) ± 1.5 (standard deviation) years in age. The study was approved by the ethics committee of the National Institute for Physiological Sciences. None of the participants reported a history of neurological/psychiatric disorders or any other contraindication to tDCS.

2.2. tDCS

The current was applied using a DC-Stimulator (Eldith), which stopped instantaneously when the resistance exceeded 13 kΩ, in order to avoid possible adverse effects. Because the resistance of the human head is largely affected by the skin condition, the skin was first wiped with gauze soaked in alcohol before the electrodes were attached. Rubber electrodes (1 mm thick) covered by a sponge (3 mm thick), which were soaked in normal saline, were attached above the ears, as shown in figure 1(a). This configuration was employed to hold both electrodes in place with a single belt around the head, simplifying the experiment and reducing human errors. The cerebral structure under the electrodes was the secondary somatosensory cortex (S2), which is important for somatosensory and pain perception. A previous study showed that tDCS over S2 yields an improvement in tactile discrimination performance (Fujimoto *et al.*, 2016). Thus, the configuration of electrodes might be useful for treatment of patients with sensory deficits. This potential advantage in clinical application made us decide to apply tDCS just above the ears in the present study.

During the stimulation, the current amplitude was increased linearly to 2 mA in the first 15 s and kept constant for 600 s. After the stimulation, the current was decreased gradually for 15 s.

doi:10.1088/1361-6560/61/24/8825

During the stimulation, the current, voltage, and resistance were recorded every 0.5 s. The resolution of the recorded resistance was within 0.1 kΩ. The same procedure was applied to measure the resistance between the rubber electrodes connected directly without a sponge.

2.3. Equivalent Circuit Model of tDCS System

A computational analysis was conducted for a multiscale model consisting of (i) the head without the skin layer and (ii) detailed layers of skin.

The resistance of the human head is used as a metric for safety. It was considered as a series circuit comprising the skin and the remaining head resistances. This assumption is valid because of the linearity of Maxwell's equations and the high resistance of the skin, which prevented the direct current flow from one electrode to the other; rather, the current flow was almost perpendicular from the head surface (e.g., Miranda *et al.* (2006)). The initial measured resistance of the two electrodes (robber and sponge) in direct contact was in the range of 1.5 kΩ to 1.8 kΩ and varied within 0.1 kΩ during the 600 s, suggesting that we can treat the electrodes with a sponge as a lumped element for an injection current of 2 mA. The equivalent circuit model for the system under consideration can be represented as shown in figure 2.

The skin resistance has nonlinear characteristics. However, for a current injection up to 100 $\mu A/cm^2$, the resistance is almost constant (Yamamoto and Yamamoto, 1981). Also, the skin resistance may depend on time because of the osmotic dehydration caused by the saline solution in the sponge (Egawa *et al.*, 2007; Egawa and Kajikawa, 2009). This will be discussed further in Sec.4.

2.4. Numerical Head and Skin Models

A macroscopic analysis was conducted using anatomically based human head models with a

resolution of 0.5 mm. At this resolution, the skin cannot be appropriately evaluated. Therefore, a separate simplified skin model with a resolution of 50 μm was considered in a microscopic analysis. Some microscopic discussion on skin modeling can be found in (Huclova *et al.*, 2011; Schmid *et al.*, 2013); also the electromagnetic modeling of the skin is listed as a topic to be resolved by IEEE International Committee on Electromagnetic Safety (Reilly and Hirata, 2016). Twenty-four head models with a resolution of 0.5 mm comprising 10 anatomical tissues were constructed from magnetic resonance images as described in Laakso *et al.* (2015). The reason for this is to discuss the variability of the head resistance, especially for internal morphology. Electrodes (50 mm × 50 mm) were attached to the head models, as shown in figure 1(a). The skin was not modeled in the macroscopic analysis. As discussed in Laakso *et al.* (2015), the scalp thickness did not have a statically significant effect on the electric field in the brain.

The simplified skin model used in the microscopic analysis is shown in figure 1(b), in which the skin pores, comprising hair follicles and sweat ducts, were modeled approximately. Its impedance is an independent element of the circuit model of the tDCS system in figure 2. The thicknesses of the epidermis, dermis, and subcutaneous fat were 50 μm or 100 μm, 2 mm, and 0.5 mm, respectively. The horizontal dimensions were 45 mm × 45 mm. The diameters of the hair follicles and sweat ducts were 50 μm (the same to model resolution) with spatial densities of 1–2 per mm^2 and 7–9 per mm^2, respectively. Three models were considered: the hair follicles and sweat ducts filled with (a) saline and (b) tap water, as well as (c) the hair follicles filled with hair, where sweat ducts are assumed as air. The locations of hair follicles and sweat ducts were determined randomly.

In the analysis of the skin resistance, the bottom of the model was truncated by a perfect conductor to compute the resistance of the skin layer. The electrode size was assumed to be 10 mm × 10 mm, which is smaller than that used in the measurement, because of the limitations on

the computational memory. However, the resistance was extrapolated for the electrode size of 50 mm × 50 mm using the inverse relationship between resistance and area.

For the analysis of the thermal computation, a fat layer of 10 mm of thickness was added to compute the temperature elevation appropriately.

2.5. Volume Conductor Modeling

Electric field dosimetry was conducted separately for the macroscopic and microscopic models. In the regime where the displacement current can be neglected, the volume conductor model is often used to investigate the internal electric field in biological tissue not only for tDCS but also for transcranial magnetic stimulation (Laakso and Hirata, 2012b; Lu and Ueno, 2015; Cvetkovic *et al.*, 2015). The scalar potential finite difference method (Dawson and Stuchly, 1998) is used to solve scalar potential equation

$$\nabla(\sigma\nabla(\phi)) = 0 \qquad (1)$$

where ϕ and σ denote the scalar potential and tissue conductivity, respectively.

By defining scalar potentials (unknowns) at each node of a cubic voxel (minimum component of the model, 9.1×10^6 voxels in this study), a branch current flowing from one node to a neighboring node along the side of the voxels was derived, which included a scalar potential due to the applied electric charge and impedance between the nodes. By applying Kirchhoff's current law at all the nodes, simultaneous equations were then set. The potential was solved iteratively using the successive-over-relaxation method and multigrid method (Laakso and Hirata, 2012b). Possible numerical uncertainties were minimized by smoothing the conductivity contrast between adjacent tissues, including the high contrast between follicles or sweat ducts and surrounding medium (Laakso and Hirata, 2012c).

The electric field along the edge of the voxel was obtained by dividing the difference in the

potential between the nodes of the voxel by the distance across the nodes and adding the vector potential. The number of multigrid levels was six, and the iteration continued until the relative residual was less than 10^{-6} (Laakso and Hirata, 2012a); for this residual, the error relative to the maximum internal electric field was less than 0.5%.

The specific energy absorption rate was calculated as

$$SAR = \frac{\sigma}{\rho}|E|^2 \qquad (2)$$

where ρ denotes the mass density of the tissue.

The head tissue conductivities are shown in Table 1(a) (supplementary material in (Laakso *et al.*, 2015). The epidermis (stratum corneum) and dermis in Table 1 (b) were taken from Yamamoto and Yamamoto (1976). The average epidermal stratum corneum was interpolated to direct current (6.6×10^{-6} S/m). The conductivity of dermis (innermost keratin layer) was 0.003 S/m. The conductivities of tap water (in Japan) and hair were taken from HoribaLtd. (1996) and van Orden (1998), respectively. The conductivity of tap water may vary by a factor of 2 (~0.03 S/m) (Torrents *et al.*, 2001). The highest uncertainty was attributed to the value for the dermis, which had not been reported until now (except as the skin). Thus, assuming that the conductivity of dermis was between epidermis and subcutaneous fat, the uncertainty analysis was assumed for the values from 0.003 S/m to 0.03 S/m (approximately the average conductivity of the epidermis and fat). The conductivity of dermis in Yamamoto and Yamamoto (1976) was similar to skin conductivity presented in (Gabriel *et al.*, 1996).

For our computation, a current source was applied between the two electrodes. The resistance was then calculated as the electric potential difference between the two electrodes divided by the applied current, which is one of the main metrics used for validating the computational results hereinafter. The resistance of the human head is often used as a metric for the side effects.

Physics in Medicine & Biology
J. Gomez-Tames *et al*
Post-Print Version
doi:10.1088/1361-6560/61/24/8825

2.6. Thermal Modeling

Thermal modeling for tDCS safety is limited (Datta *et al.*, 2009b). We conducted thermal dosimetry only for the skin-layer model (microscopic model). The temperature in the human model was calculated by numerically solving the following bioheat equation (Pennes, 1948), which considers various heat exchange mechanisms, including the heat conduction, blood perfusion, and resistive heating:

$$C(\mathbf{r})\rho(\mathbf{r})\left(\frac{\partial T(\mathbf{r},t)}{\partial t}\right) = \nabla\cdot K(\mathbf{r})(\nabla T(\mathbf{r},t)) + \rho(\mathbf{r})SAR(\mathbf{r}) + Q(\mathbf{r},t) - B(\mathbf{r},t)(T(\mathbf{r},t) - T_B(\mathbf{r},t)) \quad (3)$$

where T, K, and C are the temperature, thermal conductivity, and specific heat of the tissue, respectively; T_B is the blood temperature (37 °C); Q is the metabolic heat generation; B is the parameter associated with the blood perfusion; and $\mathbf{r}$ is the position vector.

Equation (3) was subjected to the following boundary condition:

$$-K(\mathbf{r})\frac{\partial T(\mathbf{r},t)}{\partial n} = H\times(T_s(\mathbf{r},t) - T_e(t)) \quad (4)$$

where H, T_s, and T_e denote the heat-transfer coefficient, surface temperature of the tissue, and temperature of the air, respectively. The boundaries of the side and the bottom of the skin layer model (figure 1(b)), where the temperature was assumed to be constant, were truncated by the approximate boundary condition. The size of the computational region was chosen large enough so as not to affect the computed temperature distribution; if the computational region was enlarged by 50%, the resultant temperature elevation around the computational region was affected by a few percent or less.

The bioheat equation subjected to the boundary condition was solved to investigate the resulting temperature elevation in the thermal steady state. Thus, the left-hand side term of (3)

was assumed to be zero. The equation was discretized using a finite- difference method and solved by applying the geometric multigrid method (Laakso, 2009).

The thermal parameters and mass densities used in the present study were mainly taken from Janssen *et al.* (2005), as shown in Table 2. The thermal parameters of the soaked electrodes were assumed to be the same as those of saline. When the electrodes were not soaked, the parameters were assumed to be those of the hair, owing to the lack of data. The heat-transfer coefficient between the model surface and air was set as 5 $W/m^2/°C$, which is the typical value at room temperature, i.e., 23°C (Fiala *et al.*, 1999). The temperature below the fat layer is assumed as 37°C. The initial condition was then derived assuming no SAR or power disposition exists.

Uncertainty factor in the resultant temperature elevation would be the blood flow in the skin, which may be affected by the pressure when attaching the electrodes. However, due to the lack of the data, this uncertainty is not discussed in this study.

3. Results

3.1. *Measured Resistance of Head and Electrodes*

The time evolution of the resistance measured during the tDCS treatment is shown in figure 3. The resistance of the two electrodes with wet sponge in direct contact was between 1.5 kΩ and 1.8 kΩ ($2R_e$), where the variability may have been caused by the pressure contact. When the two rubber electrodes were connected directly without a sponge or soakage in the water/saline solution, the maximum resistance was 0.1 to 0.2 kΩ. The higher impedance in the presence of sponge was mostly originated from the rubber-sponge interface. This was confirmed by measuring the electrode resistance of the two electrodes with wet sponge in direct contact at 10 Hz and 240 Hz. The resistance was reduced to 0.1-0.2 kΩ (similar to the two rubber electrodes).

doi:10.1088/1361-6560/61/24/8825

The measured resistance ($R_h + 2R_s + 2R_e$) had a large variability in the range of 2.8–5.7 kΩ at the initial state (t = 0), corresponding to a head resistance ($R_h + 2R_s$; excluding two electrodes) of 1.0–4.2 kΩ. The head resistance then gradually decreased during the 10 minutes of stimulation, corresponding to a head resistance of 0.4–2.4 kΩ. This decrease was 42–61% with respect to the initial resistance.

3.2. Computed Resistance for Head and Skin Models

The resistance of the 24 macroscopic head models without the skin (R_h) was calculated as 213 ± 11 Ω using a similar computational setup as described in (Laakso *et al.*, 2015). To incorporate the resistance of the skin, the multilayer skin model (figure 1 (b)) was considered. The computed skin resistances for the hair follicles/sweat ducts filled with saline, tap water, and hair are presented in Table 3. As shown in the table, the resistance of the skin was affected by the contents of follicles/ducts as well as the thickness of the epidermis. The resistance was relatively low when the follicles/ducts were filled with saline. This difference was caused by the difference in the conductivity among saline, tap water, and hair. The skin resistance was dominant in the total head resistance, which is consistent with Yamamoto and Yamamoto (1976).

The computed resistance of the head without the skin (R_h) was 213 Ω, as previously mentioned. Thus, the computed resistance of the human head with the skin (R_s, Table 3) was in the range of 729–1,443Ω for variable densities of hair follicles and sweat ducts. The computed resistance of the human head with the skin pores filled with saline solution ($R_h + 2R_s$) was estimated as 729−1,041 Ω. This falls within the range of values measured at the end of the experiment: 0.4−2.4 kΩ (see Sec 3.1). The resistance of the head with the skin pores filled with hair or tap water was calculated to be 1,157−1,443 Ω, which is within the range of values

measured at the start of the experiment: 1.0−4.2 kΩ.

3.3. Computed Electric Field and Temperature Elevation Distributions in the Skin

The electric field on the model surface is illustrated in figure 4 for the multilayer skin model with follicles/ducts filled with saline solution, tap water, and hair. As shown in figure 4(A-a), the electric field on the model with follicles/ducts filled with the saline solution (light blue grains) was rather smooth in the epidermis, and the high electric field around the electrode edges was not obvious, because of the high conductivity of the saline compared with tap water and hair. On the other hand, when the follicles/ducts were filled with hair only (figure 4(A-c)), the electric field around the edges was most evident and matched a previous finding (Miranda *et al.*, 2006). For deeper epidermis tissue (figure 4(B)), higher electric field was observed at the end tip of the follicles and sweat ducts (light blue) for saline solution due to higher current density in the high conductive follicles. In the subcutaneous fat tissue, a close electric field distribution can be found for the three configurations; however, saline produce a less symmetric field pattern.

The distribution of the temperature elevation calculated by specific absorption rate as a heat source is shown in figure 5. Figure 5(a) shows that the temperature elevation was smallest when the follicles/ducts were filled with the saline solution, and as shown in figures 5(b) and 5(c), the temperature elevation was almost identical when the follicles/ducts were filled with hair and tap water. Furthermore, the distribution of the temperature elevation differed from that of the electric field; the temperature was elevated at the centre rather than at the edges of the electrode. The temperature elevation around the electrode was marginally affected, even for an electrode with a larger horizontal dimension (see Sec. 2.3).

4. Discussion

One of the main elements of this study is that the resistance of the head was estimated using the multiscale head model (macroscopic model of the head and microscopic model of the skin), and validated with experimental measurements. Also, computational analysis of electric and thermal effects of tDCs in the skin was conducted.

The resistances of the human head without the skin were calculated and demonstrated to be 213 ± 11 Ω for 24 head models developed from MR images. As the head-model anatomy may depend on the classification algorithm, we also computed the head resistance using Japanese adult male model without the skin (Nagaoka *et al.*, 2004). A resistance of 210 Ω was obtained, which is within the standard variation of the 24 models. On the contrary, the skin conductivity is highly variable and dependent on the wetness and microscopic structure of the skin, and several measured values have been reported by different researchers (Yamamoto and Yamamoto, 1977). Thus, a model of the microscopic structure of the skin that includes follicles and sweat ducts can attain in more detail the skin impedance variability and effects in the distribution of the electric field under the electrode, as shown in figure 4.

We computed the skin resistance using a resolution of 50 μm. Even when a model with a resolution of 25 μm is used, no significant variation of the electric field distribution was observed. The mean error between different resolutions was 12.2% of the maximum electric field in each plane below the electrodes for the case of mean density and saline solution. Its effect on the skin impedance variation was 4.5%.

We confirmed that the inter- and intra-subject variability in the resistance is attributed to the skin condition, which is the main source of the head resistance, as shown in Table 3. When we empirically changed the conductivity of the dermis by one order of magnitude (see Sec. 2.3), the skin resistance changed by 15% or less, which did not affect the agreement between

experimental and computed resistance of the human head. In addition, the boundaries among the stratum corneum, epidermis, and dermis are not easily expressed, because they were rippled depending on the location. These factors may have caused the remaining variability in our computation.

The measured and computed resistances of the human head (excluding the electrodes) matched with saline and hair and saline conditions at the start and end of the experiment, respectively, where the resistance was 0.7−1.8 kΩ smaller at the end of the treatment. It is speculated that the variations in the initial resistance were caused by factors such as the resistance of the hair, condition of the skin pores (e.g., pore-clogging debris), contact condition of the electrodes with the skin, and the osmotic dehydration caused by the saline solution in the sponge (Egawa *et al.*, 2007; Egawa and Kajikawa, 2009). Also, the water content of the stratum corneum increases with the water-application time which may increase the conductivity (Egawa and Kajikawa, 2009). The reduction of the head resistance in the experiment was roughly estimated as the difference between the resistance of the skin filled with hair and saline: 152−714 Ω, derived from Table 3. This reduction is comparable to or lower than the minimum reduction of the resistance (0.7 kΩ) observed in the experiment. The good agreement between the measured and computed resistances, assuming saline-filled follicles, suggests the effectiveness of the multiscale modeling and the accuracy of our hypothesis that the reduction of the resistance was caused by the osmotic dehydration.

When the electrode was soaked in saline, the field concentration around the edge of the electrode disappeared. This change is attributed to the high conductivity of the saline compared with tap water and hair (figure 4). Thus, the field concentration at the electrode edge reported in Miranda *et al.* (2006) may not be evident for electrodes soaked in a saline solution. This finding differs from the previous conclusion, which was derived from macroscopic modeling only: less

saline produces a more uniform field distribution (Saturnino *et al.*, 2015).

The temperature elevation was at most 0.1 °C or less due to power absorption (figure 5). This marginal temperature elevation is difficult to confirm but using a thermography, the temperature distributions before and after the treatment was not almost identical, although not shown here. This temperature elevation was sufficiently small compared with 1−2 °C (ICNIRP, 1998), a reference value for the temperature elevation in human-safety guidelines (not medical equipment). It should be noted that skin damage has been reported at 43 °C, which corresponds to a temperature elevation of 7−8 °C (Hardy *et al.*, 1951). In addition, unlike the power-absorption distribution, the temperature-elevation distribution was more spread out because of the diffusion of heat (Hirata *et al.*, 2006). In our computation, the skin surface was assumed to be uniform. However, because of factors such as the existence of hair and the contact area of the electrodes, the internal electric field may not have been uniform, resulting in a concentration of the power absorption and temperature elevation.

For the resistance values of 30−55 kΩ reported in Palm *et al.* (2008), the temperature elevation at the injection current of 2 mA was estimated to be 1.2−2.2 °C, which is higher but comparable to the aforementioned threshold for thermal damage. The limitation of the thermal modeling is that the non-uniform power absorption was not considered in the electrodes, and the rubber was not modeled in the electrodes. Also, no skin lesions were observed when the electrode sponges were regularly replaced (Frank *et al.*, 2010). Another possible cause of the side effects is the chemical reaction between the electrodes and saline solution, which is discussed extensively in Minhas *et al.* (2010). Also, double layer effect between the electrode-skin interface can be considered for short pulse stimulation. However, this is outside the scope of this study, which only considered the physical aspects and for long stimulation periods. Finally, this study demonstrates the importance of considering multiscale analysis by

considering microscopic structures in the skin for field distributions near the electrode. Next step is to extend this approach to investigate its effects on brain field distribution for tDCS or other neurostimulation techniques.

5. Conclusions

A multiscale skin model was employed to calculate the resistance of the head for the first time. The electric field in the skin differed according to the medium of the hair follicles/sweat ducts. When the follicles/ducts were filled with a saline solution, the localization of the electric field around the edges of the electrode was suppressed because the follicles/ducts behaved as current paths. Our computational results suggest that, although the mechanism of the adverse effects of the tDCS treatment is unclear from the physics viewpoint, the electrodes soaked in saline solution suppressed these effects, which has not been obtained without a finer skin model. Moreover, it was confirmed that the temperature elevation in the skin due to the saline-soaked electrodes was not high enough to induce thermal damage for the typical head resistance. The low saline (low conductivity) of the electrode which was suggested to be useful for generating a homogeneous field around the electrode concluded by Saturnino *et al.* (2015) may not be appropriate considering this microscopic modeling. This computational modeling may be useful when designing and evaluating the tDCS electrodes.

References

Bikson M, Datta A and Elwassif M 2009 Establishing safety limits for transcranial direct current stimulation *Clin. neurophysiology* **120** 1033

Bikson M, Rahman A and Datta A 2012 Computational models of transcranial direct current stimulation *Clinical EEG and Neurosci.* **43** 176-83

Brunoni A R, Nitsche M A, Bolognini N, Bikson M, Wagner T, Merabet L, Edwards D J, Valero-Cabre A, Rotenberg A and Pascual-Leone A 2012 Clinical research with

transcranial direct current stimulation (tDCS): challenges and future directions *Brain Stimul.* **5** 175-95

Cvetkovic M, Poljak D and Haueisen J 2015 Analysis of transcranial magnetic stimulation based on the surface integral equation formulation *IEEE Trans. Biomed. Eng.* **62** 1535-45

Datta A, Bansal V, Diaz J, Patel J, Reato D and Bikson M 2009a Gyri-precise head model of transcranial direct current stimulation: improved spatial focality using a ring electrode versus conventional rectangular pad *Brain Stimul.* **2** 201-7

Datta A, Elwassif M and Bikson M 2009b Bio-heat transfer model of transcranial DC stimulation: comparison of conventional pad versus ring electrode. In: *Proc. Annual Int. Conf. IEEE Eng. Med. and Biol. Soc.*: IEEE) pp 670-3

Dawson T W and Stuchly M A 1998 High-resolution organ dosimetry for human exposure to low-frequency magnetic fields *IEEE Trans Mag.* **34** 708-18

Egawa M, Hirao T and Takahashi M 2007 In vivo estimation of stratum corneum thickness from water concentration profiles obtained with Raman spectroscopy *Acta Derm. Venereol.* **87** 4-8

Egawa M and Kajikawa T 2009 Changes in the depth profile of water in the stratum corneum treated with water *Skin Res. Tech.* **15** 242-9

Elsner B, Kugler J, Pohl M and Mehrholz J 2013 Transcranial direct current stimulation (tDCS) for improving function and activities of daily living in patients after stroke *The Cochrane Library*

Elsner B, Kugler J, Pohl M and Mehrholz J 2015 Transcranial direct current stimulation (tDCS) for improving aphasia in patients with aphasia after stroke *The Cochrane Library*

Fiala D, Lomas K J and Stohrer M 1999 A computer model of human thermoregulation for a wide range of environmental conditions: The passive system *J. Appl. Physiol.* **87** 1957-72

Frank E, Wilfurth S, Landgrebe M, Eichhammer P, Hajak G and Langguth B 2010 Anodal skin lesions after treatment with transcranial direct current stimulation *Brain Stimul.* **3** 58-9

Fujimoto S, Kon N, Otaka Y, Yamaguchi T, Nakayama T, Kondo K, Ragert P and Tanaka S 2016 Transcranial direct current stimulation over the primary and secondary somatosensory cortices transiently improves tactile spatial discrimination in stroke patients. *Front. Neurosci.* **10** 128:1-9

Gabriel S, Lau R W and Gabriel C 1996 The dielectric properties of biological tissues: III. Parametric models for the dielectric spectrum of tissues *Phys. Med. Biol.* **41** 2271-93

Hardy J D, Goodell H and Wolff H G 1951 The influence of skin temperature upon the pain threshold as evoked by thermal radiation *Science*

Hirata A, Fujimoto M, Asano T, Wang J, Fujiwara O and Shiozawa T 2006 Correlation between maximum temperature increase and peak SAR with different average schemes and masses *IEEE Trans. Electromagnet. Compat.* **48** 569-77

HoribaLtd. 1996 What is electrical conductivity? http://www.horiba.com/jp/horiba-advanced-techno/hatwave/vol2/f_s_dic/ (Accessed 20 Aug. 2016).

Huclova S, Erni D and Fröhlich J 2011 Modelling and validation of dielectric properties of human skin in the MHz region focusing on skin layer morphology and material composition *Journal of Physics D: Applied Physics* **45** 025301

ICNIRP 1998 Guidelines for limiting exposure to time-varying electric, magnetic, and electromagnetic fields (up to 300 GHz) *Health Phys.* **74** 494-521

Janssen F, Van Leeuwen G and Van Steenhoven A 2005 Modelling of temperature and perfusion during scalp cooling *Phys. Med. Biol.* **50** 4065

Kasahara K, Tanaka S, Watanabe K, Hanakawa T and Honda M 2011 Small skin lesion after treatment with repeated daily transcranial direct current stimulation (in Japanese) *Jpn. J. Clinical Neurophys.* **39** 24-7

Kuo M-F, Paulus W and Nitsche M A 2014 Therapeutic effects of non-invasive brain stimulation with direct currents (tDCS) in neuropsychiatric diseases *Neuroimage* **85** 948-60

Laakso I 2009 Assessment of the computational uncertainty of temperature rise and SAR in the eyes and brain under far-field exposure from 1 to 10 GHz *Phys. Med. Biol.* **54** 3393

Laakso I and Hirata A 2012a Computational analysis of thresholds for magnetophosphenes *Phys. Med. Biol.* **57** 6147-65

Laakso I and Hirata A 2012b Fast multigrid-based computation of the induced electric field for transcranial magnetic stimulation *Phys. Med. Biol.* **57** 7753-65

Laakso I and Hirata A 2012c Reducing the staircasing error in computational dosimetry of low-frequency electromagnetic fields *Phys. Med. Biol.* **57** N25-N34

Laakso I, Tanaka S, Koyama S, De Santis V and Hirata A 2015 Inter-subject variability in electric fields of motor cortical tDCS *Brain Stimul.*

Loo C, Martin D, Alonzo A, Gandevia S, Mitchell P and Sachdev P 2011 Avoiding skin burns with transcranial direct current stimulation: preliminary considerations *Int. J. Neuropsychopharm.* **14** 425-6

Lu M and Ueno S 2015 Computational study toward deep transcranial magnetic stimulation using coaxial circular coils *IEEE Trans. Biomed. Eng.* **PP** 1-

Minhas P, Bansal V, Patel J, Ho J S, Diaz J, Datta A and Bikson M 2010 Electrodes for high-definition transcutaneous DC stimulation for applications in drug delivery and

electrotherapy, including tDCS *Journal of Neurosci. Meth.* **190** 188-97

Minhas P, Datta A and Bikson M 2011 Cutaneous perception during tDCS: role of electrode shape and sponge salinity *Clinical neurophysiology: official journal of the International Federation of Clinical Neurophysiology* **122** 637

Miranda P C, Lomarev M and Hallett M 2006 Modeling the current distribution during transcranial direct current stimulation *Clin. Neurophysiol.* **117** 1623-9

Nagaoka T, Watanabe S, Sakurai K, Kunieda E, Taki M and Yamanaka Y 2004 Development of realistic high-resolution whole-body voxel models of Japanese adult males and females of average height and weight, and application of models to radio-frequency electromagnetic-field dosimetry *Phys. Med. Biol.* **49** 1-15

Nathan S S, Sinha S R, Gordon B, Lesser R P and Thakor N V 1993 Determination of current density distributions generated by electrical stimulation of the human cerebral cortex *Electroencephalography and clinical neurophysiology* **86** 183-92

Nitsche M and Paulus W 2000 Excitability changes induced in the human motor cortex by weak transcranial direct current stimulation *J. Physiology* **527** 633-9

Nitsche M A, Cohen L G, Wassermann E M, Priori A, Lang N, Antal A, Paulus W, Hummel F, Boggio P S and Fregni F 2008 Transcranial direct current stimulation: state of the art 2008 *Brain Stimul.* **1** 206-23

Noetscher G M, Yanamadala J, Makarov S N and Pascual-Leone A 2014 Comparison of cephalic and extracephalic montages for transcranial direct current stimulation—a numerical study *IEEE Trans. Biomed. Eng.* **61** 2488-98

Palm U, Keeser D, Schiller C, Fintescu Z, Reisinger E, Padberg F and Nitsche M 2008 Skin lesions after treatment with transcranial direct current stimulation (tDCS) *Brain Stimul.* **1** 386-7

Parazzini M, Fiocchi S, Rossi E, Paglialonga A and Ravazzani P 2011 Transcranial direct current stimulation: estimation of the electric field and of the current density in an anatomical human head model *IEEE Trans. Biomed. Eng.* **58** 1773-80

Pennes H H 1948 Analysis of tissue and arterial blood temperatures in the resting human forearm *J. Appl. Physiol.* **1** 93-122

Poreisz C, Boros K, Antal A and Paulus W 2007 Safety aspects of transcranial direct current stimulation concerning healthy subjects and patients *Brain Res. Bull.* **72** 208-14

Reilly J P and Hirata A 2016 Low-frequency electrical dosimetry: research agenda of the IEEE International Committee on Electromagnetic Safety *Phys. Med. Biol.* **59**

Rossi S, Hallett M, Rossini P M, Pascual-Leone A and Group S o T C 2009 Safety, ethical considerations, and application guidelines for the use of transcranial magnetic stimulation in clinical practice and research *Clinical Neurophysiology* **120** 2008-39

Roy A, Baxter B and Bin H 2014 High-definition transcranial direct current stimulation induces both acute and persistent changes in broadband cortical synchronization: a Simultaneous tDCS EEG study *IEEE Trans. Biomed. Eng.* **61** 1967-78

Saturnino G B, Antunes A and Thielscher A 2015 On the importance of electrode parameters for shaping electric field patterns generated by tDCS *Neuroimage* **120** 25-35

Schmid G, Cecil S and Überbacher R 2013 The role of skin conductivity in a low frequency exposure assessment for peripheral nerve tissue according to the ICNIRP 2010 guidelines *Phys. Med. Biol.* **58** 4703-16

Tanaka S, Sandrini M and Cohen L G 2011 Modulation of motor learning and memory formation by non-invasive cortical stimulation of the primary motor cortex *Neuropsychological rehabilitation* **21** 650-75

Tanaka S and Watanabe K 2009 [Transcranial direct current stimulation--a new tool for human cognitive neuroscience] *Brain and nerve* **61** 53-64

Torrents J, Mason T, Peled A, Shah S and Garboczi E 2001 Analysis of the impedance spectra of short conductive fiber-reinforced composites *J. Materials Sci.* **36** 4003-12

van Orden M 1998 Hair conductivity tests http://www.rafischer.com/hairtest.htm (Accessed 20 Aug 2016).

Wagner S, Rampersad S, Aydin Ü, Vorwerk J, Oostendorp T, Neuling T, Herrmann C, Stegeman D and Wolters C 2014 Investigation of tDCS volume conduction effects in a highly realistic head model *J. Neur. Eng.* **11** 016002

Webster B R, Celnik P A and Cohen L G 2006 Noninvasive brain stimulation in stroke rehabilitation *NeuroRx* **3** 474-81

Woods A, Antal A, Bikson M, Boggio P, Brunoni A, Celnik P, Cohen L, Fregni F, Herrmann C and Kappenman E 2015 A technical guide to tDCS, and related non-invasive brain stimulation tools *Clinical Neurophysiology*

Yamamoto T and Yamamoto Y 1976 Electrical properties of the epidermal stratum corneum *Medical and biological engineering* **14** 151-8

Yamamoto T and Yamamoto Y 1977 Analysis for the change of skin impedance *Med. and Biol. Eng. and Comput.* **15** 219-27

Yamamoto T and Yamamoto Y 1981 Non-linear electrical properties of skin in the low frequency range *Med & Biol. Eng. & Comput.* **19** 302-10

Physics in Medicine & Biology
J. Gomez-Tames *et al*
Post-Print Version
doi:10.1088/1361-6560/61/24/8825

Figure and Table Captions

Table 1. Conductivities of human head tissues. The same values of the fat conductivities were used for (a) macroscopic head and (b) microscopic skin-layer models.

(a)

Tissue	σ [S/m]
Blood	0.7
Bone Cancellous	0.06
Bone Cortical	0.013
Gray Matter	0.10
White Matter	0.10
Cerebrospinal Fluid	1.8
Eye (Vitreous)	1.5
Muscle	0.16
Fat	0.08

(b)

Tissue	σ [S/m]
Epidermis	6.6×10^{-6}
Dermis	3.0×10^{-3}
Fat	8.0×10^{-2}
Saline	1.4
Tap Water	1.5×10^{-2}
Hair	1.65×10^{-5}

Table 2. Thermal parameters of skin layer model.

Tissue	Thermal conductivity K [W/m·K]	Specific heat C [J/kg·K]	Blood flow B [W/(m^3·K)]	Metabolic rate Q [W/m^3]
Epidermis	0.42	3600	3687	1620
Dermis	0.42	3600	3687	1620
Fat	0.25	3000	1626	300
Tap Water	0.56	4220	0	0
Saline	0.62	4000	0	0
Hair	0.26	1000	0	0

Physics in Medicine & Biology
J. Gomez-Tames *et al*
Post-Print Version
doi:10.1088/1361-6560/61/24/8825

Table 3. Resistance [Ω] of skin layer (*Rs*) with hair follicles and duct densities of (i) lowest, (ii) averaged, and (iii) highest densities adjusted for 5×5 cm^2 of electrode size. The epidermis thickness was chosen as 50 μm and 100 μm. The calculated head resistance can be calculated by R_h+2R_s, where $R_h = 213$ Ω.

Thickness	50 μm			100 μm		
Density	Low	Mean	High	Low	Mean	High
Saline	371	349	326	414	336	258
Tap Water	485	477	472	566	553	540
Hair	490	491	492	611	613	615

Physics in Medicine & Biology
J. Gomez-Tames *et al*
Post-Print Version
doi:10.1088/1361-6560/61/24/8825

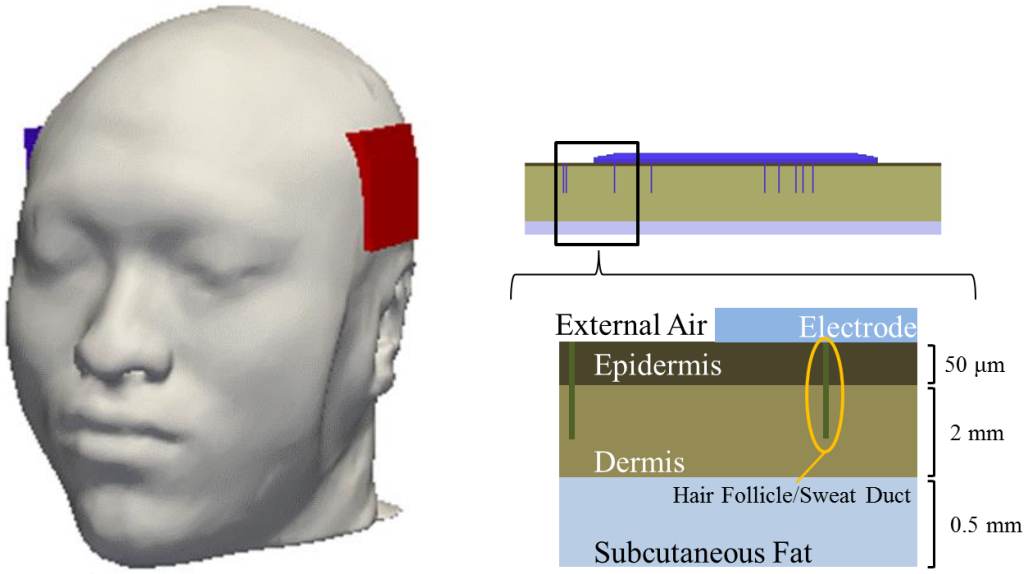

Figure 1. (a) Human head model with two electrodes attached (resolution of 500 μm) and (b) detailed skin layer model (resolution of 50 μm). The bottom of the skin model was truncated by an infinite metallic electrode.

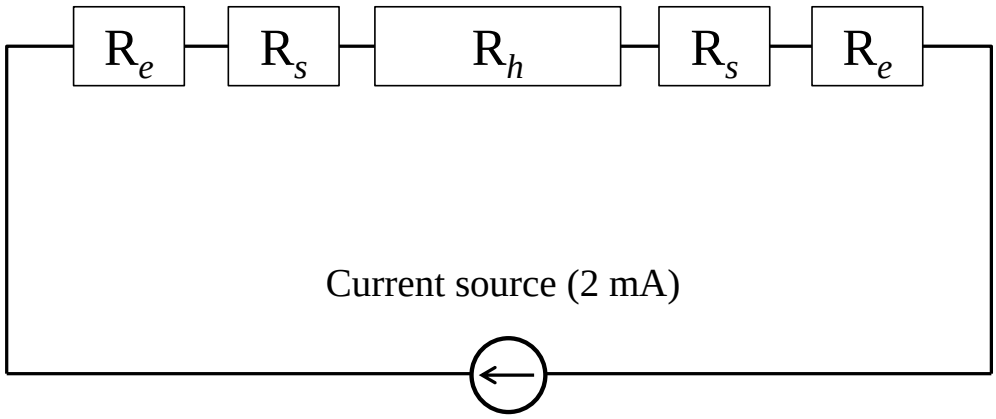

Figure 2. Equivalent circuit model of the tDCS system. R_e, R_s, and R_h are the resistance of the rubber electrode with a sponge, the skin layer (2-mm thickness), and the head model excluding the skin, respectively.

Physics in Medicine & Biology
J. Gomez-Tames *et al*
Post-Print Version
doi:10.1088/1361-6560/61/24/8825

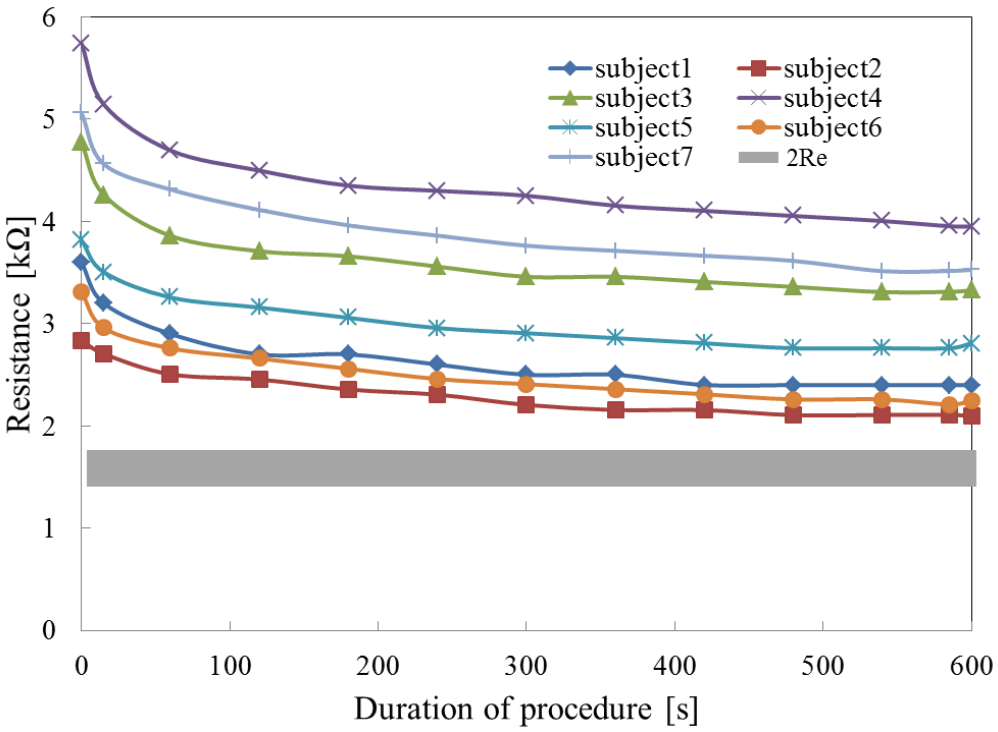

Figure 3. Resistance variation seen from the electrodes during tDCS treatment for 7 participants (Rh + 2Rs + 2Re). Variability of resistance between two electrodes (2*Re)* in direct contact is also presented to derive human head resistance (*Rh* + 2*Rs*).

Physics in Medicine & Biology
J. Gomez-Tames *et al*
Post-Print Version
doi:10.1088/1361-6560/61/24/8825

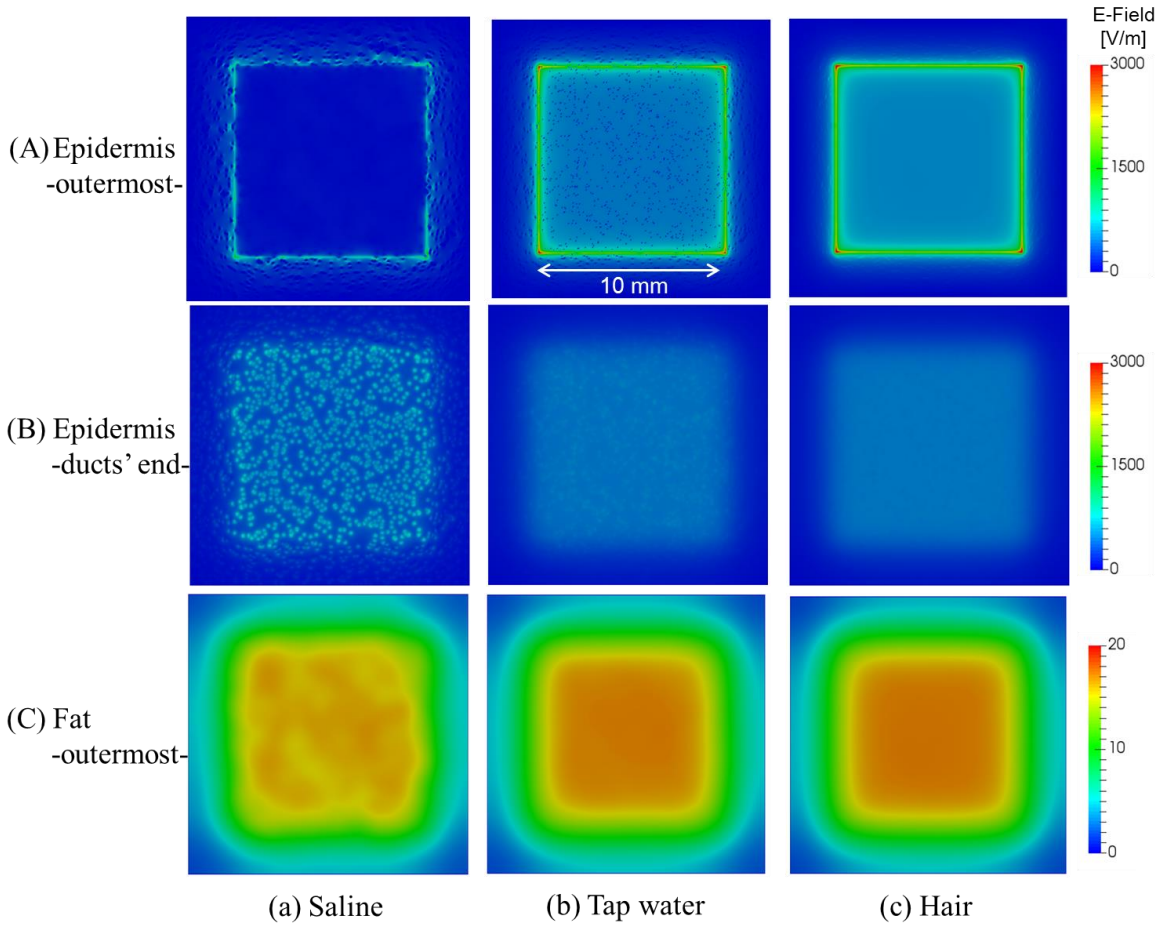

Figure 4. In-situ electric field in three locations: (A) outermost layer of epidermis (50 μm from electrode-skin interface), (B) end tip of follicles and sweat ducts (1 mm), and (C) outermost layer of subcutaneous fat tissue (2 mm) for (a) saline, (b) tap water, and (c) hair. The thickness of the epidermis is 50 μm and the maximum density of hair follicles and duct densities are used.

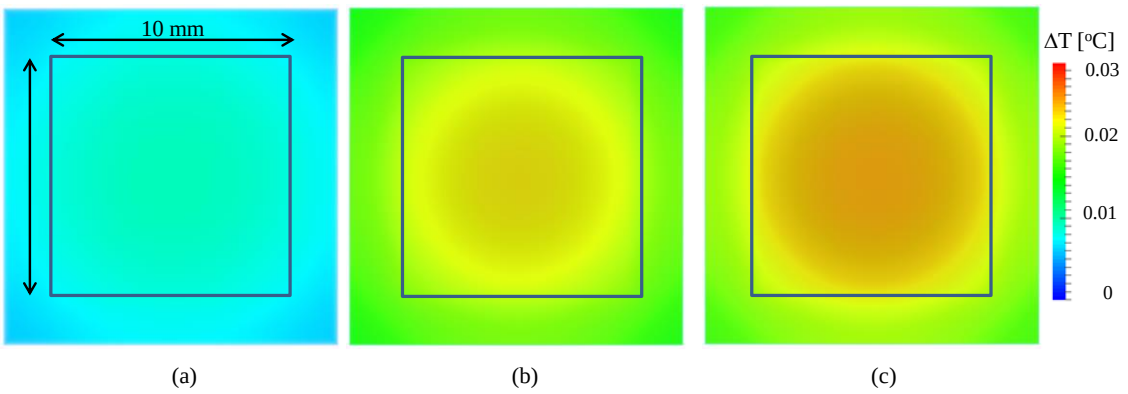

Figure 5. Temperature elevation on the epidermis for (a) saline, (b) tap water, and (c) hair. The

doi:10.1088/1361-6560/61/24/8825

dimensions corresponding to the electrode (10 mm × 10 mm) are also indicated. The thickness of the epidermis is 50 μm and the mean values of hair follicles and duct densities are used.